Proceedings Paper:
Singh, R., Bai, Q., O'Farrell, T. orcid.org/0000-0002-7870-4097 et al. (2 more authors) (2017) Concurrent, Multi-band, Single-Chain Radio Receiver for High Data-Rate HetNets. In: Vehicular Technology Conference (VTC-Fall), 2017 IEEE 86th. 2017 IEEE 86th Vehicular Technology Conference (VTC-Fall), 24-27 Sep 2017, Toronto, Canada. IEEE . ISBN 978-1-5090-5935-5

https://doi.org/10.1109/VTCFall.2017.8287876

Concurrent, Multi-band, Single-Chain Radio Receiver for High Data-Rate HetNets

R. Singh, Q. Bai, T. O'Farrell, K. L. Ford, and R. J. Langley
Department of Electronic & Electrical Engineering,
The University of Sheffield, S1 3JD, UK
Email: {r.singh, q.bai, l.ford, t.ofarrell, r.j.langley}@sheffield.ac.uk

***Abstract*—A concurrent, tunable, triple-band, single chain radio receiver for 5G radio access networks is presented and its performance is evaluated in a hardware-in-the-loop test-bed. The test-bed emulates a 5G heterogeneous network supporting three independently tunable, wideband, simultaneous connections over a frequency range from 600 MHz to 2.7 GHz. The single chain receiver is able to achieve an aggregate bandwidth of 93.75 MHz, 31.25 MHz per band, and a net data rate of 187.5 Mbit/s through the use of single-carrier QPSK transmissions. The receiver demonstrate sufficient isolation between the concurrent transmissions as well as strong resilience to adjacent blockers through the use of a small guard band.**

I. Introduction

The fifth generation (5G) of cellular mobile radio access technologies (RATs) is expected to be highly heterogeneous operating with ultra dense radio access networks (RANs) consisting of legacy and new RATs to support the ever growing demand for high data transmission rates, lower latencies and higher energy efficiencies [1][2][3]. This will require the user equipment (UE) and the base transceiver stations (BTSs) to incorporate multiple radio units, each for a different RAT, which will increase the total number of radio transceiver chains at both ends of the wireless link. This would substantially increase the size, power consumption, complexity and cost of the radio equipment in a 5G RAN [4].

Additionally, this RF bottleneck could potentially restrict the usability of a UE to one geographic region, which only allows use of specific frequency bands. Therefore, in order to meet the expectations of the 5G RAN in a compact and power efficient manner, there is a need for the development of single transceiver chain, concurrent multi-band (CM), frequency-agile radio (FARAD) units, which can enable multiple, concurrent, frequency-agile data links between the BTSs and UE. Such radio units will allow the available spectrum at any geological location to be efficiently aggregated through concurrent bands to achieve higher data transmission rates and quality of service via an always connected capability.

Direct RF digitisation can lead to frequency-agile, reconfigurable and power efficient radio front-ends [5], which have the CM transmission ability through a single transceiver chain [6]. We have proposed the design of a sub 1 GHz, concurrent, dual-band, frequency-agile radio (FARAD) receiver and tested the receiver through a hardware-in-the-loop test-bed [6]. In [??], we have proposed a concurrent, triple-band FARAD receiver with a frequency range from 0.6 GHz to 2.7 GHz. In this paper, we further characterise the concurrent, triple-band, single-chain FARAD receiver, for an increased per band bandwidth of 31.25 MHz.

The triple-band radio receiver hardware-in-the-loop test-bed utilises a tunable triple-band antenna, a digital oscilloscope, a reconfigurable triple-channel digital down converter (DDC) and baseband processing unit. The receiver is characterised based on a potential 5G RAN scenario, where a single chain CM UE receives three 31.25 MHz wide independent transmissions from three different BTSs. The receive signal quality of each data link is evaluated through error vector magnitude (EVM) measurements. In order to investigate potential interference between the bands the EVM measurements are carried out both in concurrent (all bands enabled) and individual (only one band enabled at a time) data transmission modes. The results show that there is no significant inter-band interference (IBI) between the concurrent transmissions and 93.75 MHz of aggregate transmission bandwidth can be achieved. This results in a 187.5 Mbit/s net data rate to the UE through the use of QPSK baseband modulation.

Further, an investigation into in-band adjacent channel interference (ACI) is made through the use of artificial wideband single-carrier (SC) modulated blocker signals transmitted over adjacent channels to the wanted signals. The power of the blocker signal is varied which results in -10 to +30 dB received blocker power relative to the wanted signals. The results show that the adjacent blocker signals do not affect the transmission quality of the wanted signals as long as their relative power is no more than 12 dB of that of the wanted signals. The results also show that through the use of a small guard band between the wanted and blocker signals, the receiver's EVM performance is not affected by a blocker signal with 30 dB higher power relative to the wanted signals.

II. System Description

This section provides a description of the test-bed at both the transmitter (Tx) and receiver (Rx) ends used for the characterisation of the triple-band, single chain receiver utilising the sub 3 GHz LTE bands.

A. Transmitter

A system level block diagram of the test-bed is shown in Fig. 1 (left). At the heart of the hardware-in-the-loop test-bed is the controller (PXIe-8135) [7], which is essentially

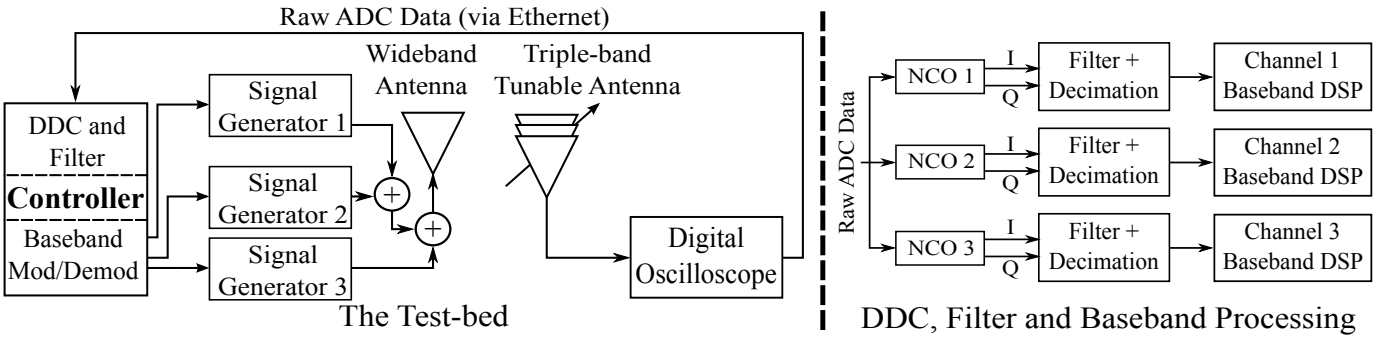

Fig. 1. Schematic of the direct RF digitising tri-band test-bed, DDC, decimation filter and baseband processing.

a PC running LabVIEW and MATLAB software packages. The baseband signal processing takes place in the controller, where three independent baseband I/Q signals are generated in LabVIEW and sent to the dedicated reconfigurable RF signal generators (PXIe-5791/5793) [8][9] operating at three distinct RF frequencies. The RF output of the signal generators is combined (ZAPD-2-272-S+) [10] and transmitted using a wideband antenna (UHALP-9108 A) [11].

B. Receiver

The RF digitising, single chain receiver comprises a tunable triple-band antenna, a digital storage oscilloscope (DSO) [12] acting as an RF digitiser, a reconfigurable triple-channel digital down-converter (DDC) and baseband processors.

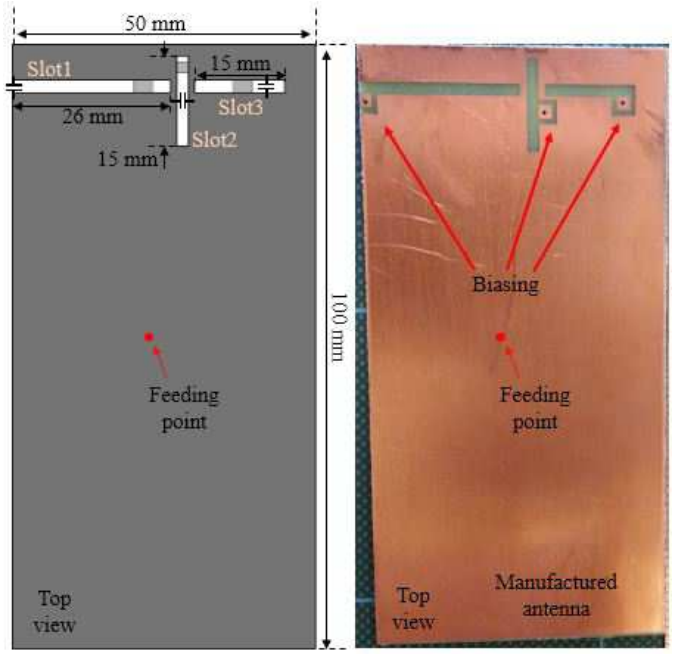

Fig. 2. Tunable tri-band antenna structure.

Tunable Tri-band Antenna: The antenna used in the receiver is an independently tunable tri-band slot antenna, which was developed from the previous tunable dual-band antenna prototype presented in [13]. The antenna is manufactured on a 50×100 mm FR4 printed circuit board (PCB), and is able to provide three concurrent and independently tunable frequency bands operating over the frequency range from 600 MHz to 2.7 GHz.

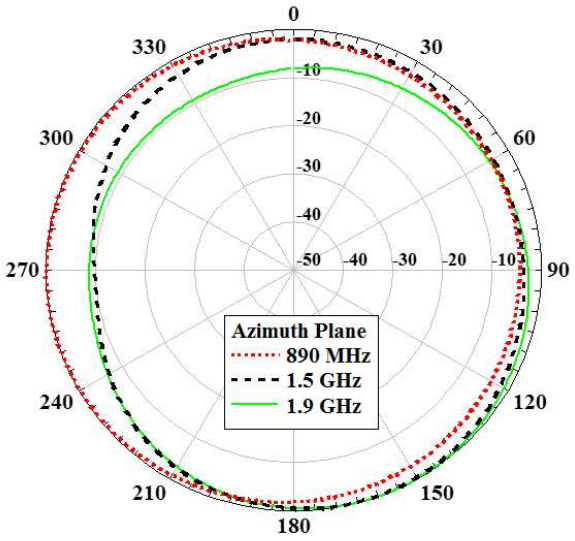

Fig. 3. Antenna azimuth radiation patterns at 890, 1500 and 1900 MHz.

As shown in Fig. 2, the antenna has three tunable slots located near the top edge of the PCB, which are used as the basic radiation elements to achieve three tunable frequency bands. Due to the limited frequency tuning range of a single slot, the total desired frequency ranges are divided into three sub-ranges: 0.6 to 1.1 GHz, 1 to 2.5 GHz and 1.9 to 2.7 GHz, which are covered by slots 1, 2 and 3 in Fig. 2, respectively. Each slot provides 35 MHz, 100 MHz and 40 MHz operating bandwidth at the test-bed frequencies 890, 1500 and 1900 MHz, respectively. The antenna azimuth radiation patterns at these three targeted frequencies are plotted in Fig. 3.

Digital Down-Conversion and Baseband DSP: The mixed RF signal detected by the triple-band antenna is directly digitised by the DSO at a sampling rate of 10 GSPS in the receiver chain. The controller acquires the digitised signal (or the raw ADC samples) from the DSO through a direct Ethernet link, before performing DDC and baseband demodulation.

The block diagram of a triple-channel DDC is shown in

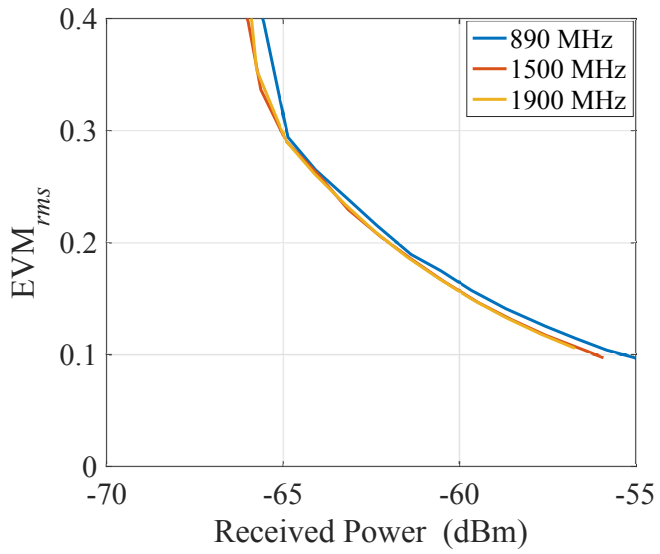

Fig. 4. EVM$_{rms}$ performance of 31.25 MHz wide *concurrent multi-band* QPSK modulated single-carrier (SC) transmissions over the tri-band test-bed.

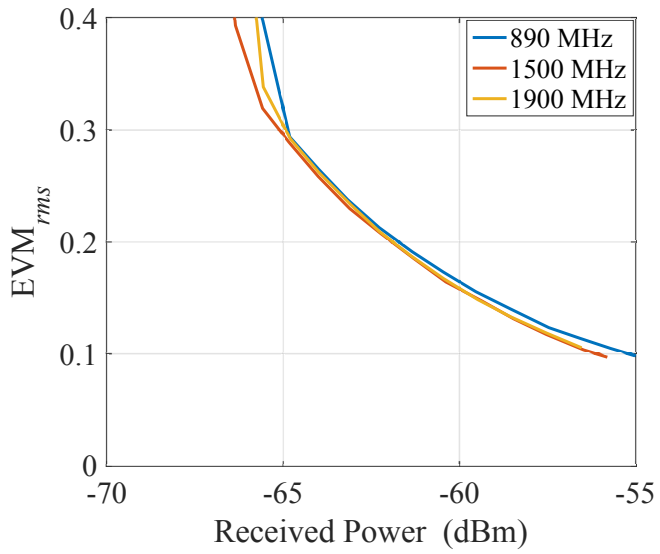

Fig. 5. EVM$_{rms}$ performance of 31.25 MHz wide *individual* QPSK modulated single-carrier (SC) transmissions over the tri-band test-bed.

Fig. 1 (right) together with the baseband processing units. DDC provides frequency conversion and decimation filtering of the desired bands before the baseband demodulation takes place. The real digital RF signal in the form of ADC samples is mixed with complex outputs of three different digital synthesisers known as numerically controllable oscillators (NCO). The DDC was implemented as a direct (or homodyne) converter. Therefore, the centre frequencies of the NCOs were set equal to the carrier frequencies of the signals generated at the Tx. This provides the baseband I/Q samples for the three concurrent channels at the receiver.

The baseband signals then pass through the cascaded integrated comb (CIC) decimation filters, which provide image and out-of-band rejection, as well as sample rate reduction to a desired level. In this work, the DDC was implemented using a MATLAB DSP function, where the NCO centre frequencies, the CIC stopband frequencies and attenuation, and the decimation factors where configured according to the bandwidths and carrier frequencies of the incoming signals. The filtered, decimated baseband signals are then processed in LabVIEW, where the timing, carrier and phase offsets are removed through the use of a synchronisation sequence and by locking to the carrier signal. Then matched filtering is performed before the *rms* EVM is estimated through equation (1) [14], where N is the number of samples received, I and Q are the ideal in-phase and quadrature levels, and $\tilde{I}$ and $\tilde{Q}$ are the received in-phase and quadrature values.

$$\text{EVM}_{rms} = \sqrt{\frac{\frac{1}{N}\sum_{i=1}^{N}(I_i - \tilde{I}_i)^2 + (Q_i - \tilde{Q}_i)^2}{\frac{1}{N}\sum_{i=1}^{N}(I_i^2 + Q_i^2)}} \quad (1)$$

III. Receiver Performance in a HetNet Scenario

A. Experimental Set-up

In this section, the performance of the presented concurrent, triple-band receiver is examined based on a potential 5G heterogeneous network (HetNet) scenario, where three concurrent, inter-band transmissions from separate BTSs are transmitted to the presented receiver (representing a UE).

The considered 5G HetNet scenario can concurrently connect a UE to a macro-cell BTS and to two small-cell BTSs. The macro-cell BTS is considered to operate at 890 MHz, whereas the two small-cell BTSs operate at 1500 and 1900 MHz, each with an instantaneous bandwidth of 31.25 MHz. The CM receiver aims to maintain similar transmission quality across corresponding radio links when operating in concurrent or individual transmission modes.

B. Results and Discussions

In order to investigate the transmission quality over each band and the IBI between the bands, three independent QPSK modulated single-carrier (SC) signals centred at the considered frequencies were transmitted (at the same power), received and analyzed through *rms* EVM evaluation. A signal bandwidth of 31.25 MHz was used for each transmission channel, yielding a total system bandwidth of 93.75 MHz and an aggregate data rate of 187.5 Mbit/s for a QPSK based transmission. Fig. 4 show the EVM vs. received power (dBm) curves for the three processed signals in concurrent transmission mode. The results in Fig. 4 show that the EVM performance of the three data transmissions are approximately equivalent. That is, over different frequency bands, the tri-band receiver achieved equivalent transmission qualities.

To establish whether or not the concurrently received signals exhibit mutual interference or IBI, the EVM performances for the same QPSK single-carrier signals were measured individually and the results are plotted in Fig. 5. The curves for

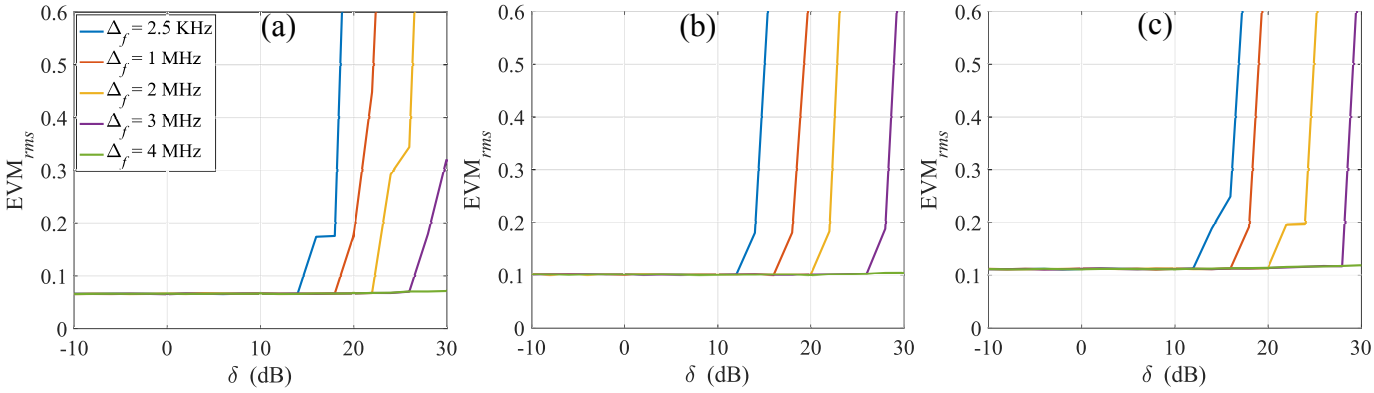

Fig. 6. The effect of in-band adjacent 31.25 MHz wide SC blockers on the EVM performance of the 31.25 MHz wide concurrent single-carrier QPSK transmissions at a) 890 MHz, b) 1500 MHz and c) 1900 MHz, with a guard band Δ_f ranging between 2.5 KHz to 4 MHz.

individually measured channels are almost identical to those for the concurrently measured channels, shown in Fig. 4. That is, the received signals in concurrent transmission mode do not experience appreciable mutual coupling when processed by the single chain receiver. Also, the rate of increase in EVM with decreasing received power is the same in concurrent and individual transmission modes.

We also investigated in-band adjacent channel interference (ACI), which can severely deteriorate the overall system performance. ACI arises due to any unwanted signals that appear at adjacent frequencies to the wanted signals. In general, such blocker signals are attenuated at the front-end by the filtering characteristics of our tunable antenna. However, as the bandwidths of each slot changes at different tuning frequencies, the adjacent blockers may interfere more unless additional filtering is considered. Further, the in-channel interference due to the spectral side-lobes of adjacent blockers cannot be filtered [15][16]. Such interference would have to be limited by ensuring a sufficient frequency gap or a guard band (Δ_f) between adjacent in-band channels.

The ACI investigation involved evaluation of EVM performance of each band in the presence of a 31.25 MHz wide QPSK SC blocker located adjacent to the wanted bands, at a minimum Δ_f of 2.5 KHz, as suggested in [17], and at wider Δ_f of 1–4 MHz. For each of these Δ_f, the power of the blocker signals was varied such that the ratio of the received power of the blocker to the received power of the wanted signals, denoted as δ, changed from -10 to +30 dB. This ratio or the relative power of the blocker signal at the receiver is defined in equation (2), where $P_{Blocker}$ and P_{Signal} are the blocker and signal average powers at the receiver, respectively. The blocker signal was generated and transmitted by a separate signal generator (SMBV100A) and wide-band antenna (UHALP-9108 A), respectively.

$$\delta = 10\log_{10}(P_{Blocker}/P_{Signal}), \tag{2}$$

The results in Fig. 6 show that none of the adjacent blocker signals will interfere with the wanted signals for up to a δ of approximately 12 dB. However, as the δ is further increased, the EVM performance of the wanted signals will degrade from ∼0.1 to be greater than ∼0.6 if no guard band is used. Therefore, use of a guard band becomes important to avoid interference from adjacent channels. The results show that for δ of up to 26 dB a Δ_f of 3 MHz each side of the wanted signal, i.e. ∼20% of the bandwidth of the wanted signals, will be sufficient to avoid any significant ACI from a wideband blocker in the current test-bed. These results show that the receiver is able to match standard specific ACI performance as the LTE release 12 also specifies that the receiver must be resilient to adjacent blocker signals with a δ of up to 25.5 dB [17].

Overall, The results show that the combined antenna and digital CIC filtering effectively prevent IBI whilst rejecting the majority of the ACI. The Δ_f requirements must be further reduced and one solution for this is the design of blocker resilient LNAs.

IV. Conclusions and Future Work

The design and data rate capabilities of a concurrent multi-band single chain radio receiver for future RANs has been explored paying significant attention to IBI and ACI. The investigations show that the receive is concurrently able to connect to three separate BTSs to achieve an aggregate bandwidth of 93.75 MHz and a data rate of up to 187.5 Mbit/s for an uncoded QPSK transmission, whilst effectively preventing IBI and ACI. The data rate could potentially be further improved through the use of higher order modulation formats, such as 64-QAM, and forward error correction techniques.

Increasing the receiver tuning range up to 3.8 GHz and performance evaluation using real world LTE-A and Wi-Fi signals are topics of future research by the authors.

V. Acknowledgement

This work was carried out in the FARAD project funded by the UK government under the EPSRC grant EP/M013723/1. The work is also supported by the UK Mobile Virtual Centre of Excellence.

REFERENCES

[1] NGMN Alliance, "5G white paper," *Next Generation Mobile Networks, White paper*, 2015.

[2] J. He, P. Loskot, T. O'Farrell, V. Friderikos, S. Armour, and J. Thompson, "Energy efficient architectures and techniques for green radio access networks," in *Communications and Networking in China (CHINACOM), 2010 5th International ICST Conference on*. IEEE, 2010, pp. 1–6.

[3] H. Hamdoun, P. Loskot, T. OFarrell, and J. He, "Survey and applications of standardized energy metrics to mobile networks," *Annals of telecommunications-annales des télécommunications*, vol. 67, no. 3-4, pp. 113–123, 2012.

[4] W. Guo and T. O'Farrell, "Green cellular network: Deployment solutions, sensitivity and tradeoffs," in *Wireless Advanced (WiAd), 2011*. IEEE, 2011, pp. 42–47.

[5] Texas Instruments, "RF Sampling and GSPS ADCs: Breakthrough ADCs Revolutionize Radio Architectures," 2012. [Online]. Available: http://www.ti.com/lit/sg/snwt001/snwt001.pdf

[6] R. Singh, Q. Bai, T. O'Farrell, K. L. Ford, and R. J. Langley, "Demonstration of RF Digitising Concurrent Dual-Band Receiver for Carrier Aggregation over TV White Spaces," in *84th Vehicular Technology Conference (VTC2016-Fall), 2016 IEEE, Accepted for Publication*, Sep 2016.

[7] National Instruments, "Embedded Controller, PXIe-8135." [Online]. Available: http://www.ni.com/datasheet/pdf/en/ds-403

[8] ——, "Embedded Signal Generator, PXIe-5793." [Online]. Available: http://www.ni.com/pdf/manuals/373949b.pdf

[9] ——, "Embedded Signal Transceiver, PXIe-5791." [Online]. Available: http://www.ni.com/pdf/manuals/373845d.pdf

[10] Mini Circuits, "Power Combiner/Splitter, ZAPD-2-272-S+." [Online]. Available: http://194.75.38.69/pdfs/ZAPD-2-272+.pdf

[11] Schwarzbeck, "Log-Periodic Antenna, UHALP-9108 A." [Online]. Available: http://www.schwarzbeck.de/en/antennas/logarithmic-periodic-broadband-antennas/standard-lpda/205-uhalp-9108-a.html

[12] LeCroy, "WaveSurfer MXs-A Oscilloscopes 200 MHz 1 GHz, 104MXs-A." [Online]. Available: http://teledynelecroy.com/japan/pdf/cata/wsxs-msxs-a-ds-12oct10-pdf.pdf

[13] Q. Bai, R. Singh, K. L. Ford, R. J. Langley, and T. O'Farrell, "Tuneable Dual-band Antenna for Sub GHz Cellular Mobile Radio Applications," in *Loughborough Antennas and Propagation Conference (LAPC), 2016 IEEE, Accepted for Publication*, Nov 2016.

[14] "IEEE Standard for Local and Metropolitan Area Networks Part 16: Air Interface for Fixed Broadband Wireless Access Systems," *IEEE Std 802.16-2004 (Revision of IEEE Std 802.16-2001)*, pp. 01–857, 2004.

[15] L. Aguado, K. Wong, and T. O'Farrell, "Coexistence issues for 2.4 GHz OFDM WLANS," in *3G Mobile Communication Technologies, 2002. Third International Conference on (Conf. Publ. No. 489)*. IET, 2002, pp. 400–404.

[16] K. Wong and T. O'Farrell, "Coverage of 802.11 g WLANs in the presence of Bluetooth interference," in *Personal, Indoor and Mobile Radio Communications, 2003. PIMRC 2003. 14th IEEE Proceedings on*, vol. 3. IEEE, 2003, pp. 2027–2031.

[17] Evolved Universal Terrestrial Radio Access, "LTE; Evolved Universal Terrestrial Radio Access (E-UTRA); User Equipment (UE) conformance specification; Radio transmission and reception; Part 1: Conformance testing (3GPP TS 36.521-1 version 12.3.0 Release 12)," 2014.